Intercomparison of Convective-Aggregation States with two Cloud Resolving Models

P. Bongioannini Cerlini[1], M. Saraceni[2], L. Silvestri[2]

[1]University of Perugia, Centro Interuniversitario di Ricerca sull'Inquinamento e sull'Ambiente Mauro Felli (CIRIAF) - Centro di Ricerca sul Clima e Cambiamenti Climatici (CRC), Perugia (PG)
[2]University of Perugia, Department of Civil and Environmental Engineering (DICA) - Centro di Ricerca sul Clima e Cambiamenti Climatici (CRC), Perugia (PG)

Key Points:

- The two models ARPS and SAM achieve a state of convective organization through different mechanism and different degree of aggregation
- The predominance of clouds-radiative or moisture-memory feedback is dependent on the initialization, microphysics and sub-cloud properties

Corresponding author: M.Saraceni, `miriam.saraceni@studenti.unipg.it`

Abstract

The Radiative-Convective Equilibrium (RCE) of two models exhibiting convective aggregation has been compared. The goal of the work, following the suggestion from the Radiative-Convective Equilibrium Model Intercomparison Project (RCEMIP), is to identify key parameters controlling self-aggregation in RCE for both models and discuss the processes controlled by these parameters in order to find the simulations similarities and to test their differences. The two models studied, the SAM (System for Atmospheric Modeling) and the ARPS (Advanced Regional Prediction System), have different physical and numerical formulations. This allowed us to compare the sensitivity to processes related to self-aggregation. When self-aggregation occurs, the two models present similar statistics for what concerns precipitation, warming, and drying of the atmosphere and anvil cloud area reduction (leading to an "Iris effect"), within the spread of the RCEMIP values. On the other hand, they differ both in the degree of organization and the organization feedback: SAM is strongly organized (is on the highest quartile of the RCEMIP for the Iorg Index) and the convective organization is achieved by cloud-radiative feedback; ARPS is weakly organized (on the multi-model average of the RCEMIP for the Iorg Index) and the moisture-convection feedback is leading to the convective organization. The prevalence of one mechanism over the other has been found in the interaction between the microphysics and the sub-cloud layer properties. This comparison suggests that, in order to have a robust measure of climate sensitivity, climate models should include both types of convective organization mechanisms as shown by the two models.

Plain Language Summary

The Radiative-Convective Equilibrium is a paradigm for atmospheric modeling of the tropics. In such a paradigm, the clustering of clouds can spontaneously occur and it can substantially affect the energy budget of the climate system. To study this phenomenon, we selected two models, with different numerics and physics, and we investigated the equilibrium statistics. We compared our results with the ones of the Radiative-Convective Equilibrium Model Intercomparison Project, where different models were used. We found similar precipitation, warming, and drying of the atmosphere, between the two models and that experiment. Instead, we found different types of cloud clusters and different feedback processes leading to this clustering. We attributed this difference to the representation of cloud formation processes in the two models and the initial properties of the layer below the clouds. This might have implications for the change in clouds with warming within the climate system.

1 Introduction

The radiative-convective equilibrium (RCE) of an ensemble of clouds has been used as a paradigm of a statistical equilibrium state of the atmosphere able to mimic the tropical part of the climate system. Given the crucial importance of moist convection inside the climate system and how to parameterize it inside climate models, RCE simulations have been used as a proxy to study the link between global circulation and convection (Held et al., 1993; Randall et al., 1994; Pauluis & Held, 2002b, 2002a). After these initial numerical studies, a number of additional studies were performed using RCE as a starting point to study the variability and organization of convection over a wide range of space and time scales. Among the different approaches used to evaluate convective variability, there was: the simulation of RCE states to study the predictability of rainfall at high resolution (Islam et al., 1993), the organization of convection (Robe & Emanuel, 1996), and the orographic variability of precipitation (Bongioannini Cerlini et al., 2005). Given the aims of these last simulations, different models were used with fixed imposed radiation and simplistic microphysical parametrization schemes, without ice phases of water content. The increased computing capability available made it possible to run three-

dimensional high-resolution simulations (Tompkins & Craig, 1998; Bretherton et al., 2005) and to study the sensitivity of RCE states using models with enhanced dimensions of the grid reaching the dimensions of mesoscale processes, with explicit moist variables and different physics parameterizations.

The characteristic that arose further the attention over the RCE simulations was the spontaneous development within these simulations of the convective organization (self-aggregation) using cloud resolving models. Such models can simulate the space-time statistics of an ensemble of clouds (Khairoutdinov & Randall, 2003) over domain sizes with spatial extension up to hundreds of kilometers and for a length of time much longer than that of a single cloud over homogeneous surface conditions. Despite the differences in parametrizations packages (e.g. microphysics, radiation, turbulence) between models, they showed in some cases spontaneous self-aggregation of clouds (Tompkins & Semie, 2017; Khairoutdinov & Emanuel, 2010; Jeevanjee & Romps, 2013; Ruppert Jr & Hohenegger, 2018; Holloway & Woolnough, 2016; Hohenegger & Stevens, 2016).

Generally, it has been pointed out that convective organization is the result of feedback between moisture-convection-radiation, which can be related to various processes (C. Muller et al., 2022; Wing et al., 2017). Bretherton et al. (2005) and C. J. Muller and Held (2012) found that a low level circulation from the dry to moist regions, forced by longwave radiative cooling in the lower troposphere, is responsible for self-aggregation, by transporting moist static energy (MSE) up-gradient. Wing and Emanuel (2014) using a MSE variance budget confirmed such a mechanism. On the other hand, C. Muller and Bony (2015) found that aggregation could be obtained by suppressing rain evaporation, even in the absence of radiative feedback. This mechanism was called "moisture-memory aggregation", where moist regions remain moist, thus more favorable to convection (Tompkins, 2001b; Craig & Mack, 2013).

Given the differences among models, the need for comparison among them, with different dynamical formulations, has been stated recently in different studies (Tompkins & Semie, 2017; Wing et al., 2017, 2018). The impact of different model representations of cloud physics and convective processes has been recognized as a key point to assess the closeness between model self-aggregation to the atmospheric convective organization and to compare the climate sensitivity to self-aggregation feedback as represented by models (Wing et al., 2020). How to assess the robustness of statistical variability and its closeness to the observed variability of tropical convection for simulations of RCE states (where convective variables show self-aggregation), is one of the reasons for the work done within the Radiative-Convective Equilibrium Model Intercomparison Project (RCEMIP) experiment. In fact, within RCEMIP, the different models used, one-dimensional, three-dimensional, and global, were driven to a radiative-convective equilibrium, using a predefined protocol to start from conditions that were as similar as possible. Despite this, since the equilibrium state is achieved in a statistical sense, and given the differences in the convection simulations of the RCEMIP models spectrum, the different sensitivity to various climatic parameters produced different results. Furthermore, it was underlined that different model responses are linked to differences in models physics and numerics (Wing et al., 2020). Thus, the question remains as to which factors in the models are prevalent in aggregation.

For these reasons, this study sets out to compare two models in their reproduction of convection statistics: The Advanced Regional Prediction System (ARPS, Oklahoma University (OU), (Xue et al., 2000, 2001)) and the System of Atmospheric Modeling (SAM) (Khairoutdinov & Randall, 2003). ARPS is a state-of-the-art reference model from its use in three-dimensional simulations based on a non-hydrostatic formulation of conservation equation for momentum, energy, and water variables used for Numerical Weather Predictions (NWP) (Xue et al., 2014; Sun et al., 2021). It is recalled here that this model, although very similar to the most common WRF model (Skamarock et al., 2005), was not included in the RCEMIP (Wing et al., 2020). Therefore, this is the first study that investigates self-aggregation with such a model.

The SAM model, based on an anelastic approximation, is formulated to conserve the liquid/ice static energy, which is a standard variable to study an ensemble of clouds that is continuously forced in a RCE simulation. Thus, SAM has been used extensively to study convective self-aggregation (Bretherton et al., 2005; Wing & Emanuel, 2014) and it is the model on which the aggregation theory was based (C. J. Muller & Held, 2012; Emanuel et al., 2014).

The objective of this paper is to see how an aggregated state of convection is achieved when ARPS is run in its standard setting and to compare it to the state achieved by the SAM model. The aggregation of convection is in fact an indication of the internal oscillation of the model in an RCE configuration that is not used in the basic model setup. This configuration, where the boundary conditions are periodic and the lateral energy transport is absent, causes the model to reproduce a statistical oscillation within the system. By reaching the statistical equilibrium of precipitation, one can study the statistical oscillation of convection within the model, and its intrinsic process of convective organization, thus comparing the dominant processes in convection in the two families of models. We want to understand what kind of processes are dominant for this type of convection aggregation and to understand how similar or different these processes are when used on tropical/global scales.

Since the ways in which convection is organized depends on both the dimensionality of the domain (C. J. Muller & Held, 2012; Patrizio & Randall, 2019) and the intrinsic characteristics of the models (Wing et al., 2020; Yang & Tan, 2020; Pope et al., 2021), it is possible that the mode of internal equilibrium of the two models analyzed may contain information about the mode of oscillation of the climate system, that combines both oscillations of the compared models. This idea comes from the results of RCEMIP, where the degree of self-aggregation in SAM-CRM is outside the multi-model spread, while the WRF-CRM one is on the multi-model average. ARPS statistic, for the listed parameters that can be compared, appears to be average with many of the models used, and distant from the SAM statistic.

Thus, the research questions posed by this study are:

- What are the statistical properties of convection when each of the models reaches a stable state?
- Is the internal oscillations leading to similar aggregation processes (in terms of the statistical stability of convection) in the two models?

In Section 2 the two models, the numerical simulation setup and the initialization are described. In Sections 3 and 4 the results of the convective organization statistics, the cloud properties, and the convective organization feedback are described and discussed. In Section 5 a summary of the work is given.

2 Numerical Simulations

2.1 The SAM model

The first simulation is performed by using the System of Atmospheric Modeling (SAM version 6.10.6, Khairoutdinov & Randall, 2003). SAM solves the anelastic continuity, momentum, and scalar conservation equations. The prognostic thermodynamic variables are the total non precipitating water ($q_T = q_v + q_c + q_i$ = water vapour + cloud water + cloud ice), the total precipitating water ($q_p = q_r + q_s + q_g$ = rain + snow + graupel) and the liquid/ice static energy, $h_L = c_pT + gz - L_v(q_c + q_r) - L_s(q_i + q_s + q_g)$, with L_v and L_s being the latent heat of vaporization and sublimation, respectively. By definition, h_L is conserved during the moist adiabatic processes (including freezing/melting of precipitation).

Given h_L, q_T and q_p, the mixing ratio of the various hydrometeors (q_c, q_i, q_r, q_s, q_g) is diagnosed by partitioning relationships that depend only on temperature. The di-

agnosed mixing ratios are used to compute the water sedimentation and hydrometeor conversion rates through a bulk microphysics scheme, where the autoconversion of cloud water into rain is evaluated through the Kessler scheme, while ice aggregation is parametrized similarly to Lin et al. (1983). Cloud ice is considered as non-precipitating water but it is allowed to fall with its own terminal velocity $V_{TI} = 0.4$ m/s (Khairoutdinov & Randall, 2003).

Longwave and shortwave radiative fluxes are computed using the radiation code from the National Center for Atmospheric Research (NCAR) Community Atmosphere Model (CAM version 3.0, Collins et al., 2006).

We choose a first-order Smagorinsky closure scheme for subgrid-scale (SGS) turbulence. The same SGS parametrization was used in previous studies by Bretherton et al. (2005); C. J. Muller and Held (2012); Wing and Emanuel (2014). Surface fluxes are interactively computed according to the Monin-Obukhov similarity theory.

2.2 The ARPS model

The second simulation is performed by using the Advanced Regional Prediction System (ARPS version 5.3.4, Xue et al., 2000, 2001). ARPS solves the fully compressible conservation equations for mass, momentum, heat, and water substance (water vapor, liquid, and ice). The thermodynamic prognostic variables are the potential temperature, pressure, and the mixing ratio for six water species (water vapor, q_v, cloud water, q_c, cloud ice, q_i, rain, q_r, snow, q_s and hail,q_h).

Precipitation is computed through a bulk microphysics scheme where autoconversion of cloud water into rain is evaluated through the Kessler scheme (Kessler, 1969) and ice aggregation is treated with the three ice categories (cloud ice, snow, and hail or graupel) scheme of Lin et al. (1983).

The radiation code is adopted from the NASA/Goddard Space Flight Center, with shortwave radiative fluxes based on the model of Chou (1990) and longwave radiative fluxes based on the model of Chou and Suarez (1994). Surface fluxes are computed according to the Monin-Obukhov similarity theory and a first-order Smagorinsky scheme has been chosen for turbulence closure.

Table 1. Main properties of the two numerical models and simulations: the model version; the horizontal resolution, Δx; the size of the squared domain; the initial sounding used to start the run (see Figure **??**); the total running time; the radiation, microphysics, sub-grid scale mixing and surface fluxes parametrizations.

	SAM	ARPS
Model version	6.10.6	5.3.4
Δx (km)	3	3
Domain size (km)	768	1152
Initial sounding	SND-301 (Figure **??**)	SND-296 (Figure **??**)
Run time (days)	160	158
Radiation (Fully interactive)	CAM version 3.0 (Collins et al., 2006)	NASA/ Goddard (Chou, 1990; Chou & Suarez, 1994)
Microphysics	Original SAM single-moment (Khairoutdinov & Randall, 2003)	Warm-rain Kessler scheme (Kessler, 1969), Ice Lin scheme (Lin et al., 1983)
Subgrid-scale mixing	First-order Smagorinsky	First-order Smagorinsky
Surface fluxes (Fully interactive)	Monin Obukhov similarity	Monin Obukhov similarity

2.3 Numerical setup and initialization

The SAM simulation is performed over a doubly periodic domain with size 768 × 768 km^2 and a uniform horizontal resolution of 3 km. We use 64 vertical grid levels with a rigid lid at the top at about 27 km. The first level is at 25 m and grid spacing gradually increases from 50 m near the surface to 500 m above 5 km. Then, it increases again from 500 m to 1 km above 20 km. Newtonian damping is applied to all prognostic variables in the upper third of the model domain (above 18 km). At the bottom, there is an oceanic surface with a constant sea surface temperature of 302 K, which is usually considered as the lower limit for self-aggregation to happen (Wing & Emanuel, 2014). The simulation is run with fully interactive radiation as done in Stephens et al. (2008); C. Muller and Bony (2015); Ruppert Jr and Hohenegger (2018). There is no mean wind and no rotation.

The ARPS simulation has a horizontal resolution of 3 km, with a large domain of 1152 km in length. We use 62 vertical levels with a rigid lid at the top at about 25 km. The first level is at 35 m and grid spacing is 35 m up to 140 m. Then the vertical grid is gradually stretched from about 70 m to about 700 meters up to 20 km. Above 20 km the grid spacing is about 800 m. Rayleigh damping is applied above 19 km. The simulation is run with fully interactive radiation, no mean wind, no rotation, and with an oceanic surface at a constant SST of about 302 K.

The main properties of numerical models and simulations are summarized in Table 1. Both simulations run for about 160 days. SAM runs with a time step of 10 s, while ARPS run with a time step of 6 s. Output fields are generated every 6 hours. The SAM simulation is initialized with a sounding obtained from a previous run of the SAM model in RCE equilibrium without self-aggregation (SND-301, see Supplementary Figure S1a). Convection is initiated by adding white noise to h_L in the lowest five levels, with an amplitude of 0.1 K in the lowest level linearly decreasing to 0.02 K in the fifth level.

ARPS is initialized with a colder and drier profile (SND-296, see Supplementary Figure S1b) which is obtained by running an 80-days simulation over a small domain (96 km x 96 km). This smaller simulation was initialized with the SND-301 profile. The new initialization profile, SND-296, is obtained by averaging mean temperature and water vapor on the smaller domain over the last 10 days, when statistical equilibrium is reached. Convective motions are initialized by applying a random perturbation of magnitude 0.2 K to the potential temperature field over the whole domain.

The initial colder and drier profile of ARPS turns out to be crucial for later stages of convective aggregation. Therefore we briefly introduce here some elements leading to the decrease in temperature and humidity of the ARPS domain. A more in-depth discussion will be provided in Section 4. Figure 1a shows the non-aggregated state of the small domain simulation after 75 days. Precipitable water (Figure 1b) drops very quickly from about 60 mm to 42 mm, while the daily precipitation rate exhibits an opposite behavior by increasing abruptly to about 6.5 mm/day (Figure 1b). After a few days of simulation, the small domain is entirely covered by a very thin anvil cloud which remains there until the end of the simulation (Figure 1c). The average cooling and drying of the ARPS domain are due to the presence of such an anvil which blocks the incoming solar radiation. Such high cloud fraction over small domain simulations of RCE has been found also during the RCEMIP project by Wing et al. (2020) (see Figure 9 in the article) and therefore it is not related only to the specific model configuration. When initializing the large domain ARPS simulation (following the RCEMIP protocol by (Wing et al., 2018)), the cloud water and ice at 12 km, produced by the smaller domain, are removed (Figure 1c), removing the large anvil, while leaving its effect on the vertical profile of temperature and water vapor. Therefore convective motions of ARPS start in a drier and colder domain than those in SAM.

The main mechanisms behind the anvil formation in the ARPS small domain rely on the properties of the microphysics scheme adopted by the model, as mentioned in the previous section. Further details are provided in Section 4.

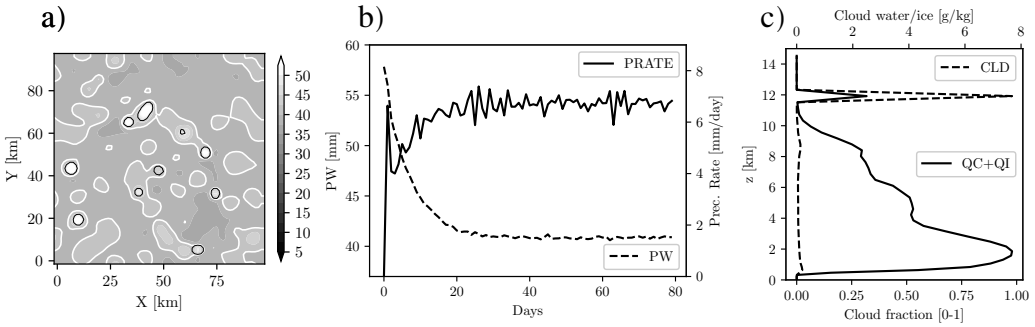

Figure 1. Snapshots of PW at day 75 (midnight) on the small domain used to initialize ARPS simulation (same contours and colors used in Figure 2) (a). Time evolution of daily averaged precipitation rate and precipitable water over the ARPS small domain (b). Cloud fraction and total cloud condensate averaged over the last 20 days of the small domain simulations (c).

3 Results

3.1 Statistics of convective organization

In SAM and ARPS simulations The precipitation rate reaches a statistical equilibrium, with similar values of 4.2 $mm\ day^{-1}$ in SAM and of 4.1 $mm\ day^{-1}$ in ARPS. The domain average statistics of the simulations final stages are reported in Table 2. In SAM, a RCE state is reached, where the Total Heat flux (THF, sum of the latent heat flux LHF and sensible heat flux SHF) is in balance with net column radiative cooling (R_{NET}), and the LHF, which dominates the THF, is in balance with precipitation (Precip) (see Table 2). In ARPS, instead, the net atmospheric energy imbalance, F_{NET}, is greater than in SAM ($F_{NET} = 4.16\ Wm^{-2}$), reaching a value similar to that obtained for the model WRF in RCEMIP (see Table 2).

Both model simulations present the convective organization as it is shown by the Precipitable Water (PW) pattern evolution in Figure 2. The convective organization is marked by the clustering of convection, as underlined in Figures 2d and 2h for ARPS and SAM respectively, when precipitation equilibrium is reached. There is a marked intensely convecting moist patch surrounded by a region of dry subsiding air (Bretherton et al., 2005).

By looking at the evolution of the two simulations, it can be noted that in SAM the convective organization is achieved with the expansion of dry regions, with suppressed precipitation, that seclude a moist region where convection occurs. In ARPS, such expansion is not as evident as in SAM.

In SAM, the PW pattern is uniform until the 40th day, when a dry patch at x = 400 km starts to form (see Figure 2f and the *Homvöeller* diagram of the PW in supplementary Figure S2a). Between days 40-80, the system evolves into an organized state, with the dry patch covering most of the domain at the equilibrium (after day 100). In ARPS, instead, the PW pattern is uniform until day 20 when some moist patches and two dry patches form at x = 400 km and x = 800 km (see Figure 2b and the *Homvöeller* diagram of the PW in supplementary Figure S2b). By day 60 the moist regions converge into a single moist patch when the equilibrium state is reached, with a moist region surrounded by a drier region (see also Supplementary Figure S2b).

There is a difference between the dimensions of the developing convective clusters. Regarding SAM, the dry zones are very large compared to the moist zone, where convection is taking place, covering almost the 90% of the whole domain (Figure 2h). The convective cluster in SAM has a diameter of nearly 300 km. For ARPS instead, the or-

Table 2. RCE average statistics over the aggregated state (days 135-140) of simulations, following Table A2 of Wing et al. (2020). The values for the RCEMIP SAM-CRM model, RCEMIP WRF-CRM model, and the average (± the standard deviation) of RCEMIP models are reported in the last three columns for a direct comparison. Such values are directly taken from Table A2 or the text of Wing et al. (2020). $\mathbf{F}_{NET}$ is the atmospheric energy imbalance, that is the magnitude of the difference between R_{NET} and the total surface thermal fluxes; R_{NET} is the column integrated atmospheric radiative forcing (negative values indicates net atmospheric radiative cooling) which is obtained directly by column integration of the radiative forcing (qrad, prognostic variable); LHF and SHF are surface latent and sensible heat (positive values indicates fluxes into the atmosphere); PW is the precipitable water; Precip. is the daily precipitation rate; LWP and IWP are the cloud liquid water path and cloud ice water path respectively. LR is the tropospheric (15 km) Lapse Rate; T_s, RH_s are respectively the absolute temperature and the relative humidity at the lowest model level.

Var	Unit	SAM	ARPS	RCEMIP-SAM	RCEMIP-WRF	RCEMIP-AVG (STD)
$\mathbf{F}_{NET}$	W m^{-2}	4.16	26.15	3.87	21.73	4.12 (±5.66)
R_{NET}	W m^{-2}	-122.80	-102.46	-118.05	-106.54	-110.17 (±16.08)
LHF	W m^{-2}	120.26	65.46	113.15	90.37	101.93 (±15.29)
SHF	W m^{-2}	6.71	10.85	8.77	37.90	11.16 (±5.74)
PW	mm	25.7	38.1	31.2	41.2	32.8 (±4.1)
Precip.	mm day^{-1}	4.2	4.1	3.9	3.1	3.5 (±0.5)
LWP	mm	0.056	0.015	0.048	0.065	0.041 (±0.028)
IWP	mm	0.015	0.001	0.025	0.097	0.037 (±0.038)
LR	K km^{-1}	-6.68	-7.08	-7.2	-6.91	-6.83 (±0.65)
T_s	K	300.3	298.4	n/a	n/a	n/a
RH_s	%	64	75	n/a	n/a	73 (n/a)
Iorg		0.9	0.6	0.9	0.5	0.6 (n/a)

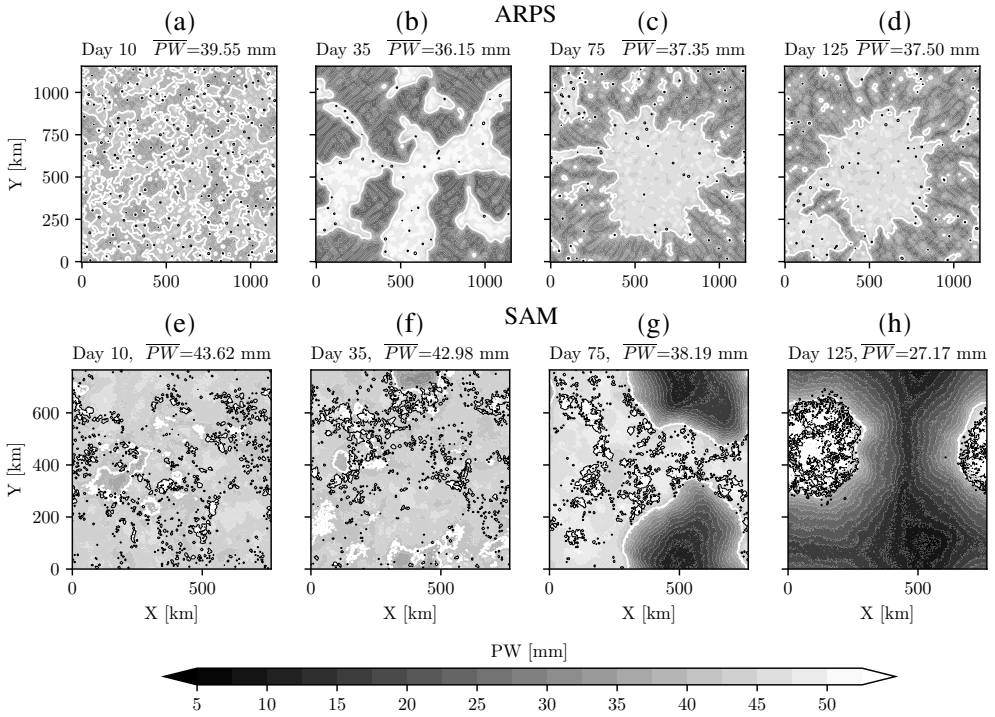

Figure 2. Time evolution of Precipitable Water (PW, filled contours) for ARPS (a,b,c,d) and SAM (e,f,g,h) simulations. The region where aggregation occurs is moister and presents a higher PW (lighter colors). For both models snapshots are taken on midnight after 10 (a,e), 35 (b,f), 75 (c,g) and 125 (d,h) days. The thick white line represents the boundary between moist and dry patches, taken as PW=40 mm. Black lines are contours of total water condensate of 0.4 g/kg at a height of 1.5 km, representing low-level clouds. It is important to recall here the different scales on the X and Y-axis.

ganization of convection comes with dry areas that cover near the same percentage of the moist areas, with 40% of the simulation domain covered by the convective cluster, which has a diameter of approximately 550 km (Figure 2d). The greater domain size of ARPS could have influenced this percentage, by allowing the formation of multiple clusters (as is evident in Figure 2d), as it has been found in previous studies (Stephens et al., 2008; Wing et al., 2018; Patrizio & Randall, 2019).

The difference underlined by PW patterns can be further explained by looking at the moisture sorted time series of the Water Vapor Path (WVP) (Figure 3). These are computed by dividing the two simulations domain into blocks of equal area (96 km^2), and then sorting them into four quartiles from driest to moistest, based on their daily WVP.

Figure 3a shows that while in SAM there is a very large inter-quartile difference, especially between the driest and moistest quartiles, in ARPS this difference is smaller. Indeed, for SAM, as in (Bretherton et al., 2005), the driest WVP quartile is the one that decreases most dramatically from day 25 until day 75 by about 27 g/m^2, when the organization is developing, while the moistest quartile increases in WVP of about 3 g/m^2. Instead in ARPS, the moistest and driest quartiles seem to be 5 g/m^2 higher and 5 g/m^2 lower than the WVP domain daily mean respectively, after organization occurs (Figure 3b).

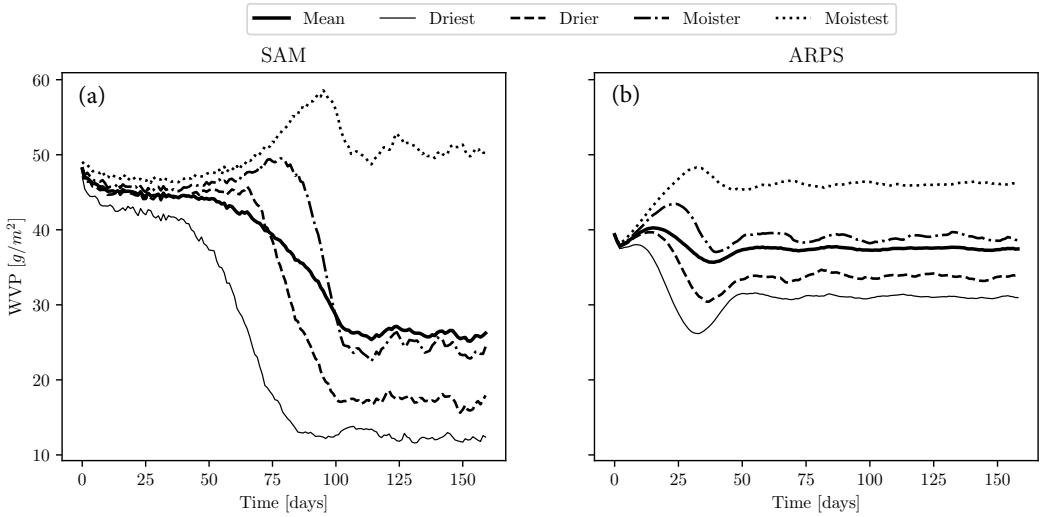

Figure 3. Moisture-sorted time series of the daily averaged Water Vapor Path (WVP) g/m^2 for SAM (a) and for ARPS (b). The thick lines are the domain mean and the other curves are the means over the 96 km^2 blocks sorted into four quartiles based on their daily WVP.

In both SAM and ARPS, WVP increases only in the quartiles where deep convection is taking place and decreases in the dry regions. This is also reflected by the precipitation quartiles (not shown), in which after aggregation has occurred, the moister and moistest quartiles present precipitation, while in the driest and drier quartiles, it is absent. However, the equilibrium is reached in both models, where the whole system reaches its statistical equilibrium, and the PW oscillates around a mean value (Figure 4d).

Convective organization in both SAM and ARPS has the same impact on the simulated atmosphere, leading to its warming and drying, as it is reported in Figure 4a 4b and 4c. The warming produced by the organization process can be inferred from the mean state profiles of MSE, Temperature (T), and Relative humidity (RH) averaged at equilibrium (between 135-140 days) over the whole domain with respect to the initial ones (averaged between the first 5-10 days).

In fact, in the case of SAM, we notice a decrease of MSE in the lower troposphere (around 2 km), due to the general drying of the atmosphere, and growth of MSE in the upper troposphere due to warming (Figure 4a). In ARPS, on the other hand, it can be seen that the MSE profile is initially dryer than the SAM one and remains dry in the lower troposphere, while it warms up at equilibrium with an MSE growth occurring in the mid-troposphere. The warming is underlined by the increase in temperature (Figure 4b) in both simulations, while the drying can be noted in Figure 4c with the relative humidity decreasing in the whole troposphere in both simulations, and in Figure 4d where the PW is shown to decrease with the organization in both SAM and ARPS.

These results are in line with the main results of the RCEMIP (Wing et al., 2020) who found that there is a robustness of the results on heating and drying of the mean state with convective organization among models. The temperature and relative humidity profiles of both SAM and ARPS are within the ensemble spread of RCEMIP mean state profiles (see Figures 7 and 8 of (Wing et al., 2020)). However, SAM final state is warmer and drier than the ARPS one (Figure 4). This is also evident from the values at the surface shown in Table 2, which are near the RCEMIP range values. The surface relative humidity (RH_s) is 64% for SAM and 75% for ARPS and the surface temperature (T_s) is 300.3 K for SAM and 298.4 K for ARPS. As already stated in the previ-

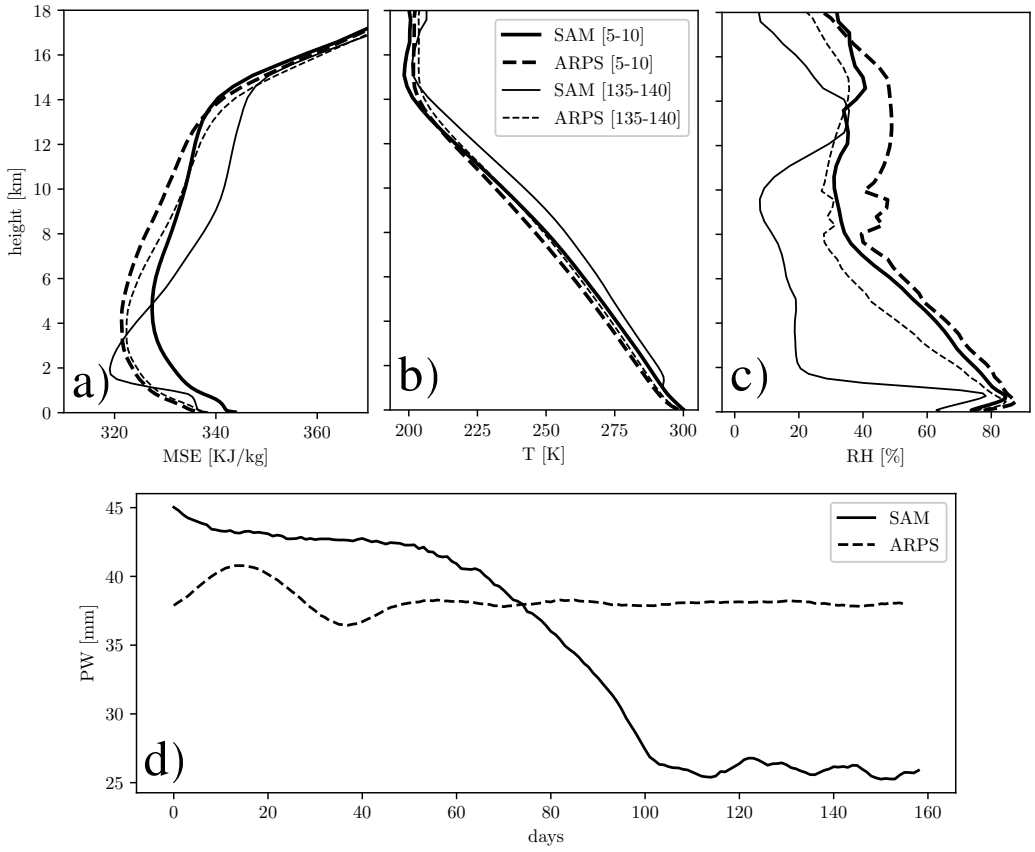

Figure 4. Horizontally averaged profiles of Moist Static Energy (MSE) (a), absolute Temperature (T) (b), and Relative Humidity (RH) (c) for the two simulations, averaged at the initial stage (5-10 days) and at the final aggregated state (135-140 days). Time evolution of Precipitable Water (PW) for both simulations (d). Precipitable water is evaluated by considering all condensates.

ous section, given the different initialization, ARPS starts already with an initial colder profile compared to SAM.

The warmer and drier final state of SAM is reflected also in the values of the surface fluxes (see Table 2). Given the smaller RH_s in the SAM model, the LHFs are larger (LHF = 120 $W\ m^{-2}$) than those of ARPS (LHF = 65 $W\ m^{-2}$). On the other hand, given the smaller T_s of ARPS, the SHFs are larger (SHF = 11 $W\ m^{-2}$) than those of SAM (LHF = 7 $W\ m^{-2}$). The same behavior is observed by comparison with the RCEMIP results from WRF and SAM models (see Table 2).

Regarding the state of the convective organization degree in the two models, we have decided to compute the Organisation index (Iorg) (Tompkins & Semie, 2017), which is shown in Figure 5a. It is a measure of the convective organization, which compares the nearest neighbor distribution of convective cores of the simulated and random convection. In ARPS it reaches an averaged daily value of 0.6 at equilibrium, a value much lower than the one of 0.9 attained by SAM at equilibrium. This is in agreement with the results of the RCEMIP project (Wing et al., 2020), where similar values were found for both models (see their Figure 12). The Iorg value reached by ARPS is closer to the average value of the multi-model comparison in RCEMIP (mean value of 0.6, see Table 2), while SAM is in the highest quartile among the models. Based on such metrics, we can

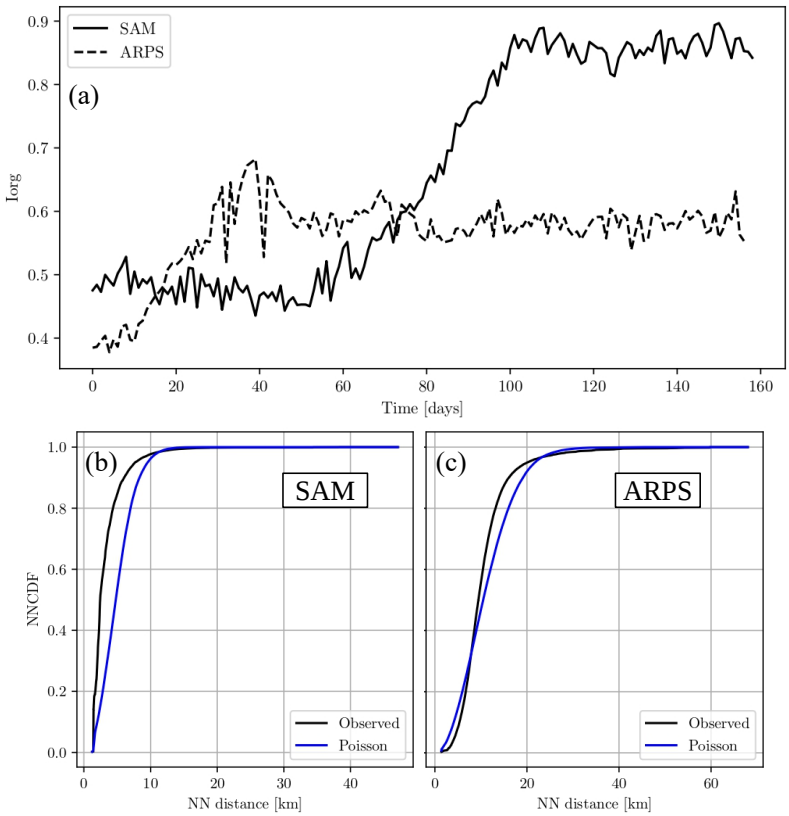

Figure 5. The daily Organization index (Iorg) for SAM and ARPS, as computed by (Tompkins & Semie, 2017) is reported in (a), while the corresponding cumulative density function of the calculated Nearest Neighbor distances (NNCDF) versus nearest neighbor distance of observed and idealized Poisson convective distribution is displayed for SAM in (b) and for ARPS in (c).

infer that SAM undergoes a strongly organized convection, while in ARPS the organization is weaker (Figure 5a).

The Iorg evolution mirrors the evolution of the PW (Figure 4d) and that of the WVP (Figure 3). Interestingly, between days 35-40 in ARPS, the Iorg index oscillates, reaching its maximum value of 0.7. This corresponds to a decrease in PW, caused by an expansion of dry patches and a corresponding clustering of moist regions (see Supplementary Figure S2b).

The observed cumulative density function of the calculated Nearest Neighbor distances (NNCDF) in ARPS (Figure 5c) indicates the presence of regular convection at distances less than 10 km, while the clustering occurs at larger spatial scales, up to 60 km. This regular convection is noticeable also in Figure 2c and Figure 2d, where shallow clouds are regularly distributed over the domain. A similar distribution was obtained from WRF-RCE simulations (Tompkins & Semie, 2017) and also from satellites observations of tropical convection (Semie & Bony, 2020). This regular convection is absent in SAM (Figure 5b), where the clustering of convection occurs immediately at very small spatial scales. Indeed, in Figure 2h only one cluster is present, made by very small and packed convective structures.

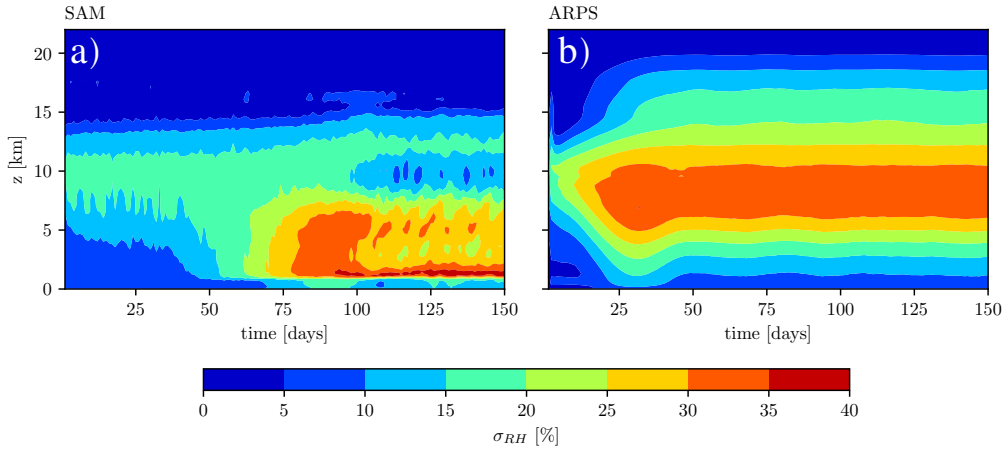

Figure 6. Temporal evolution of the domain averaged standard deviation of relative humidity (σ_{RH}) for the SAM (a) and ARPS (b) simulation.

3.2 Cloud properties

The evolution of the convection variability can be followed by looking at the domain averaged standard deviation of the relative humidity (σ_{RH}), as shown in Figure 6. After the initial time steps, there is a relevant perturbation at 10 km that amplifies in both models. Convection is occurring immediately after the initialization, starting from the middle troposphere, thus slightly increasing the σ_{RH} there. Then, for SAM (Figure 6a), after 75 days, the σ_{RH} starts increasing – reaching a value of around $\sigma_{RH} = 40$ % – in the lower to middle troposphere (from 1.5 km to 7.5 km), as deep convection organizes. Instead, for ARPS, the initial perturbation starts expanding to all troposphere after 10 days, and then, after 25 days, the increase of σ_{RH} reaches its maximum in the middle troposphere, at 7.5 km with a value of $\sigma_{RH} = 35$ %, as convection organizes. Similar results to ARPS have been found in (Tompkins & Semie, 2017) for the WRF model.

From this analysis, it can be inferred that, although the convective organization is occurring in the two models, the type of convection is different. If in SAM the σ_{RH} increases especially in the lower troposphere, in ARPS this happens in the mid-troposphere, thus convection is located at different heights in the two models.

The difference in the cloud properties in the two models is underlined in Figures 7a, 7b, 7c and 7d, which show respectively the radiative forcing, the cloud fraction, the cloud water and the cloud ice at the initial stage (averaged between 5-10 days) of the considered simulations. As adopted in RCEMIP (Wing et al., 2020), a cloud is defined according to a threshold value of cloud condensate ($10^{-}5$ kg kg^{-1} or 1% of the saturation mixing ratio over water, whichever is smaller).

The cloud fraction profiles at the initial state are very different among the two simulations, especially regarding the high-level clouds (> 8 km). This is also visible in Figure S3, where anvil clouds evolution is shown. The peak high cloud fraction ("anvil") is very large for ARPS: the ARPS anvil is located at 12 km and reaches an average value of cloud fraction of 0.9, and the cloud fraction is equally distributed between 10 and 15 km. On the other hand, SAM simulation develops an anvil with a much smaller average cloud fraction of 0.13 at 12 km height. (Khairoutdinov et al., 2022) showed that the single moment microphysics of SAM, as used in this article, underestimates the amount of high cloud. This is also visible from our results, where the high cloud fraction is much less than in the ARPS model, where different microphysics is used. The major difference in the microphysics parameterization between the two models is the presence of ice

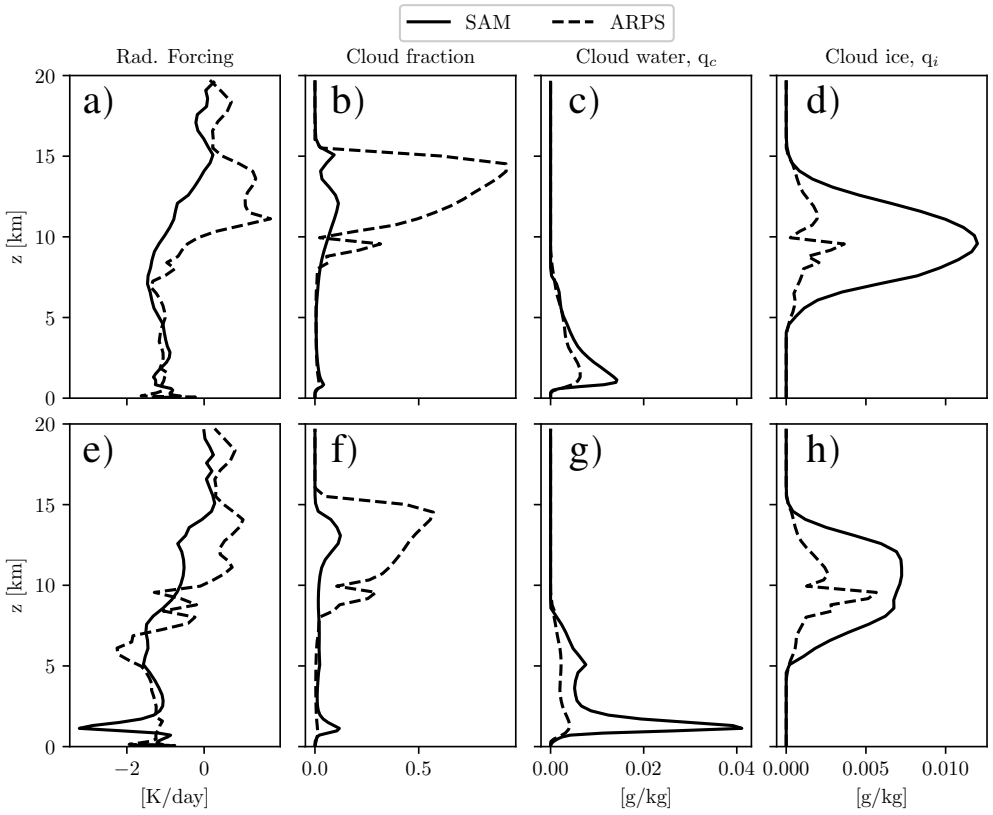

Figure 7. Radiative forcing, cloud fraction, cloud water, and cloud ice for the initial state (a,b,c,d) and the final state (e,f,g,h) of the two simulations. The initial (final) state is averaged over the days 5-10 (135-140) days for both simulations.

sedimentation, which in SAM is permitted, with an ice terminal velocity of 0.4 m/s. In Khairoutdinov and Randall (2003) it was verified that the presence of ice sedimentation in SAM leads to a reduced anvil below 9km. Thus, in the absence of ice sedimentation, the anvil in SAM would have been more extensive.

The thick anvil of ARPS heats the upper troposphere, while it cools the middle and lower troposphere (Figure 7a). In SAM there is cooling in all troposphere except for the top of the anvil at 15 km. This is because ice cirrus clouds act to reflect incoming short-wave radiation and entrap long-wave radiation from the clouds below (Liou, 1986; Schlimme et al., 2005). In both models, especially in ARPS, the effect of anvil clouds on the radiative heating profile is to warm near the cloud base and cool near the cloud top, as pointed out by (Hartmann & Berry, 2017).

With the convective organization, the anvil cloud fraction is greatly reduced both in ARPS and SAM as is shown in Figure 7f, while the low cloud fraction notably increases only in SAM. The presence of low clouds in SAM has been considered a necessary factor for convective organization (C. J. Muller & Held, 2012; Wing & Emanuel, 2014; C. Muller & Bony, 2015), which increases with increasing resolution (Khairoutdinov et al., 2009). In general, the presence of low clouds in RCEMIP models is highly variable and presents a strong spread among CRMs in the mean state. The presence of low clouds in SAM compared to ARPS may be related to the formation of downdraft and in general to the temperature profile reached by the two models, as will be discussed in more detail in the following sections.

Indeed, at the top of the boundary layer, SAM presents a simulated cloud fraction slightly higher than ARPS, with a cloud cover fraction > 0.1 and a higher content of q_c (q_c = 0.015 g/kg for SAM and q_c = 0.009 g/kg for ARPS). Then, the cloud water increases drastically in SAM with aggregation, with an equilibrium value of 0.04 g/kg, while in ARPS is slightly reduced (Figure 7g). The cloud ice decreases in SAM, almost by half, while increases in ARPS, reaching a value of 0.005 g/kg (Figure 7h). This is probably related to the ice to snow different conversion threshold used in the models microphysics scheme, being higher for ARPS than for SAM.

The correspondent radiative forcing in SAM is a pronounced cooling at 2 km of almost -4 K/day (see also the radiative forcing quartiles in Supplementary Figure S4). This marked cooling is absent in ARPS simulation because low clouds are too few and the cloud water is low. Around 6 km height, ARPS show a larger radiative cooling than that of SAM (Figure 7e). Such cooling comes mainly from the dry regions (see Supplementary Figure S4). One possible reason behind the difference between the SAM and the ARPS mid-tropospheric cooling is to be found on the different anvil properties. Ticker anvils are more efficient in blocking the removal of heat in the convective region, with respect to dry regions. Thus, a larger amount of heat must be transported to the dry regions and radiated out to space (Wing et al., 2017; Yang & Tan, 2020).

The spatial difference in cloud fraction between the two models is also shown in Figure 2, where the black dots represent the low clouds. In SAM the presence of low clouds is significant from the beginning of the simulation and increases with the organization of convection (Figure 2e and Figure 2h), while in ARPS the low clouds decrease with aggregation (Figure 2a and Figure 2d).

3.3 Convective organization feedback

The convective organized state in SAM is characterized by the onset of a virtual circulation of MSE from the dry to the moist regions (C. J. Muller & Held, 2012). The mesoscale circulation that develops with the organization can be visualized using the stream function Ψ (Bretherton et al., 2005), derived as the horizontal integral over vertical velocity starting from the driest column to the moistest, after having sorted them from lowest to highest Column Relative Humidity (CRH). The same sorting described in the previous section 3.1 is applied here, but in this case, it is done based on the CRH. By looking at the advective tendencies of MSE, implied by the stream function, one can capture the general mechanism of energy exchange between the columns. In SAM, the MSE "circulation" is imposed between the moist and dry columns only after the 50th day (not shown). By day 100, SAM has attained a state of convective organization. An up-gradient transport of MSE is visible (Figure 8a), with the low MSE being accumulated in the dry columns. In the moistest blocks (40-64) there is an inflow in the lowest level (1-2 km), while the outflow is mainly between 8 to 10 km. These fluxes are in correspondence with the presence of a deck of low clouds (Figure 8a).

This is in accordance with what is underlined in the equilibrium state sorted mass flux (taken as $M = \rho w$ with units of $kg\ m^{-2}s^{-1}$). Indeed in SAM, there is a pronounced updraft in the moist region at 1.5 km with the downdraft occurring in the moister and drier column (Figure 9c). Once convective aggregation has been imposed in the simulation, the sorted quartiles become divergent, compared to the initial days (Figure 9a).

In the dry quartiles there is a strong radiative cooling at the top of the moist boundary layer generated by low-level clouds, which drives subsidence (see Figure 7e and Supplementary Figure S4). The simulation shows pronounced cooling only at the top of the low clouds, formed in the moist columns. As C. J. Muller and Held (2012) has highlighted, this cooling generates subsidence in the dry regions, and the mid-level warming enhances the upward motion in the moist regions. The former induces a horizontal convergence of air from the moist columns to the subsidence top area, the latter instead corresponds to an upward flux raised by surface heat fluxes. To close the circulations a lateral inflow of dry air develops from dry columns to moist columns at low elevation (1 to 1.5 km).

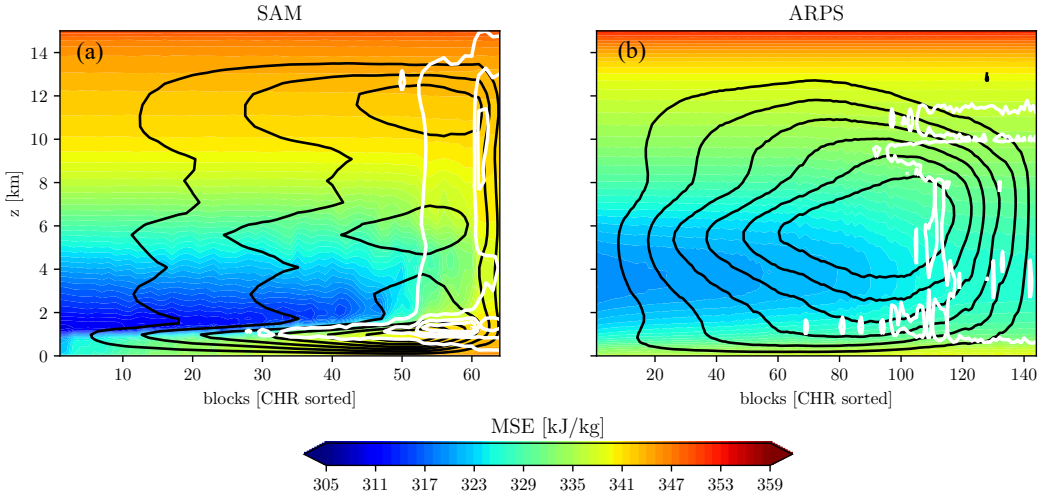

Figure 8. The average value of the MSE "circulation" between 135-140 days for SAM (a) and ARPS (b), with columns ranked by Column Relative Humidity (CRH), from driest to moistest. Black contours show the stream function Ψ (contour interval 0.05 $kg\ m^{-2}s^{-1}$, starting at 0.01 $kg\ m^{-2}s^{-1}$, solid for positive values and dashed for negative values) as a function of CRH and height. White contours show cloud condensate (cloud ice and cloud water) $q_N = q_i + q_c$ (contour interval 0.005 g/kg, starting at 0.001 mg/kg). Shaded contours represent MSE.

This circulation advectively diverges MSE out of the driest columns, increasing the MSE gradient.

This low-level cooling is purely attributable to longwave cooling produced by the presence of low clouds, as previously recognized in the literature (C. J. Muller & Held, 2012; Wing & Emanuel, 2014; C. Muller & Bony, 2015). The low clouds, as stated also in the previous sections, are of primary importance for the onset of aggregation. By looking at Figure 8a one can see that they reach more than half of the sorted blocks, while the SAM anvil at equilibrium occupies only the moistest ones.

Emanuel et al. (2014) demonstrated similar feedback in a two-layer model where the phenomenon of self-aggregation is regarded as the result of the linear instability of the RCE state, which leads to deep convection and upward motion in part of the domain and dry air with few clouds in the rest, reconciling the stable equilibria of Sobel et al. (2007). The instability happens when a negative moisture perturbation leads the dry columns to become dryer, owing to an increased longwave cooling and the consequent downward motion. In the moist columns, a positive moisture perturbation leads them to enhance their upward motion by decreasing the long-wave cooling.

In ARPS, on the other hand, the "circulation" of MSE is not noticeable, both in the days before the organization (not shown) or once the simulation has reached the organized equilibrium (Figure 8b). There is no sign of circulation below 2 km (as also noticeable in Figure 9d). Instead, there are updrafts in the moist regions, reaching their maximum at around 8 km, and downdrafts in the dry regions (see Figure 8b). This, rather than being a sign of the up-gradient transport of MSE, is a result of the occurrence of ARPS convective towers in the moist regions with downdrafts at the edges of these regions and in the remaining part of the dry domain. Also in Figure 8b, it can be seen the absence of low clouds covering the domain (as already pointed out in previous sections), as well as the greater size of the ARPS anvil compared to that of SAM.

The fact that the low-level circulation never appears in ARPS is also demonstrated by looking at the bottom layer wind speed at the boundary between the moist and the

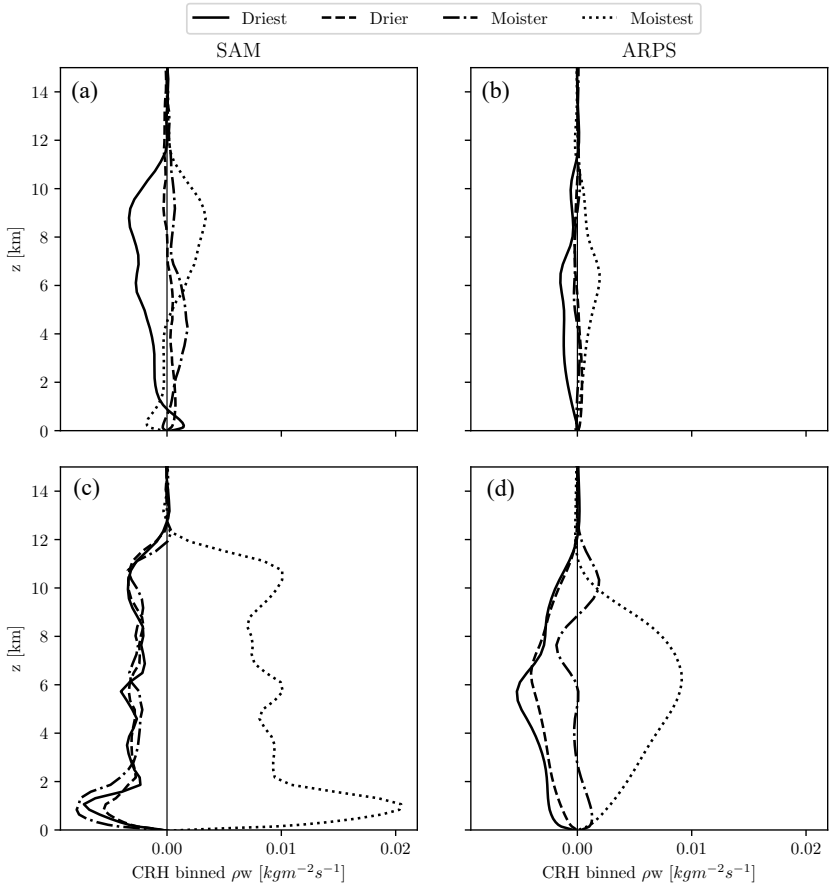

Figure 9. Average values of the CRH blocks-quartiles binned of the mass-weighted vertical velocity between the 5th and the 10th day for SAM (a) and ARPS (b), and between the 135th and the 140th day for SAM (c) and ARPS (d).

dry regions (see Figure 10c). While in SAM such velocity increases (which is a clear signal of a radiatively driven aggregation as shown by Windmiller and Craig (2019), see their Figure 8), in ARPS it remains almost constant. Thus, rather than being a convective organization led by radiative feedback, there must be other processes at play in the ARPS model.

Indeed, C. Muller and Bony (2015) found another type of aggregation called "moisture-memory aggregation", which is favored by weak downdrafts below clouds. Weak downdrafts can occur when the sub-cloud layer is nearly saturated and rain cannot evaporate. Figures 10a and 10b show that ARPS has a saturated sub-cloud layer both at the start (not shown) and at the end (Figure 10a) of the simulation. Instead, SAM never reaches such condition (Figure 10b). The saturation of the sub-cloud layer in ARPS directly influences the downdrafts properties: ARPS downdrafts are weaker than those in SAM and they cover a smaller fraction of the domain (see Supplementary Figure S5). This again does not favor the radiative aggregation which is mostly sustained by downdrafts induced by the radiative cooling above shallow clouds.

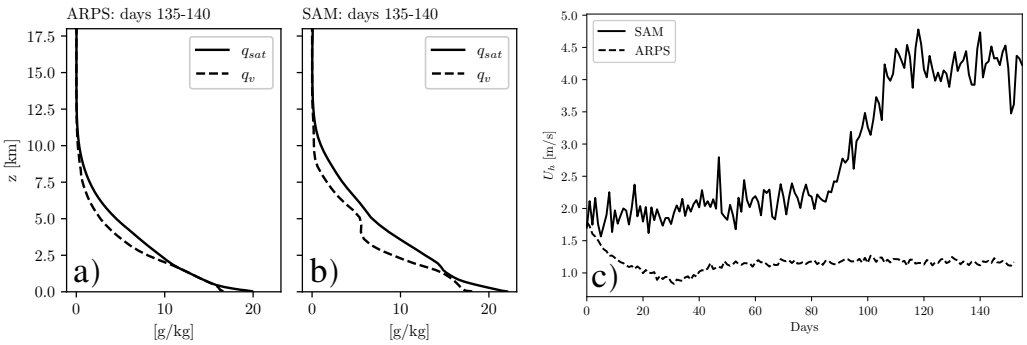

Figure 10. Vertical profiles of ARPS saturation water vapor mixing ratio (q_{sat}) and water vapor mixing ratio (q_v) over cloudy grid points (defined as grid points at 1.5 km height where the total cloud water condensate exceeded 10^{-3} g/kg) between days 135 and 140 a); b) same as a) but for SAM simulation; time evolution of bottom layer horizontal wind speed (U_h) averaged over the boundary between moist and dry patch (identified with the same criterion as in Figure 2) c).

4 Discussion

In the literature, (C. Muller & Bony, 2015; C. J. Muller & Held, 2012; Wing & Emanuel, 2014; Tompkins & Semie, 2017; Coppin & Bony, 2015) many experiments have been carried out in order to assess the sensitivity of convective organization to different choices of physical parameters and processes within the same CRM. Here we wanted to study the same robustness of the convective organization process found within the same model, by using two different models. In particular, we recognize different physical mechanisms leading to the convective organization in the ARPS and SAM model.

In general, the SAM model undergoes a "radiative aggregation" (Emanuel et al., 2014), where the MSE up-gradient circulation, driven by the contrasting radiative cooling rates between the moist and the dry regions, is the main driver of convective aggregation (C. J. Muller & Held, 2012). On the other hand, the organized state in the ARPS model does not exhibit such MSE circulation (Figure 8), but it can be traced back to a "moisture-memory aggregation" (C. Muller & Bony, 2015; C. Muller et al., 2022) or moisture-convection feedback (Tompkins, 2001b).

C. Muller and Bony (2015) found a similar result within the SAM model, by weakening the effect of cold pools. In particular, the moisture memory aggregation was favored by weaker downdrafts below clouds, which can occur when the sub-cloud layer is nearly saturated and rain cannot evaporate. Such condition has been verified in ARPS by looking at the profiles of the water vapor saturation mixing ratio (Figure 10), where the sub-cloud layer is saturated between 1 and 2.5 km both at the start and at the end of the simulation. SAM never reaches such conditions due to the higher temperature throughout the troposphere and, hence, a greater saturation mixing ratio. The saturation of the sub-cloud layer in ARPS causes less rain evaporation, weaker downdrafts, and a weaker cold pool effect than those in SAM. Another signal of a weaker cold pool effect is the weaker surface fluxes in ARPS, compared to those in SAM (see Table 2). As shown by (Tompkins, 2001a; Schlemmer & Hohenegger, 2014; Drager & van den Heever, 2017), gusty wind brought by cold pools generally enhance surface fluxes. The weakening of cold pools has been generally proven to favor convective aggregation (Jeevanjee & Romps, 2013; C. Muller & Bony, 2015) through the moisture-memory feedback: moist regions remain moist and thus become more favorable to convection since downdrafts are not able to suppress deep clouds.

Moreover, radiative aggregation and the MSE up-gradient circulation are not favored in ARPS by the smaller amount of shallow clouds (and also a smaller domain fraction covered by downdrafts). On the contrary, the SAM model exhibits a larger amount of low clouds with a strong radiative cooling at their top (Figure 7). This creates the so-called "radiatively-driven" cold pools (Coppin & Bony, 2015) and the downdrafts which initiate the low-level circulation of MSE. Low clouds are sensitive both to domain horizontal resolution and size (C. J. Muller & Held, 2012; C. Muller & Bony, 2015) and also to the downdrafts strength (Khairoutdinov et al., 2009). Lower resolution and smaller domain size have been found to decrease the number of shallow clouds in SAM (C. Muller & Bony, 2015). Such argument was used to explain why self-aggregation does not occur below a certain resolution and domain size. Khairoutdinov et al. (2009) showed that removing the evaporation of rain in their simulation (thus weakening cold pools), also results in a lower shallow cloud fraction covering the domain. In this case, new deep clouds were found to develop at the sites of previous deep clouds, resembling the moisture-memory feedback. When rain evaporation was present, deep clouds tended to appear along the edges of spreading cold pools, favoring also the formation of shallow clouds.

Therefore, the convective organization can occur even with a low amount of shallow clouds and weak MSE circulation, once it is ensured that the sub-cloud layer is enough saturated to weaken downdrafts (Wing et al., 2017). Different sub-cloud layer properties can arise spontaneously from different models even when starting from a similar setting as in the RCEMIP project (Wing et al., 2018). Indeed, Wing et al. (2020) found a substantial spread in the domain average temperature and humidity profiles after reaching equilibrium.

Differences in the way the convective organization is achieved in CRM, by using other models than SAM, have been noticed in previous studies (Jeevanjee & Romps, 2013; Yang & Tan, 2020; Tompkins & Semie, 2017; Holloway & Woolnough, 2016). For example, Holloway and Woolnough (2016) found that a low level circulation was present in the Met Office Unified Model, but was driven mainly by anomalies in low-level diabatic heating from convection and other microphysical processes, and not by radiative cooling gradients between the moist and dry regions. Furthermore, they found that this wasn't a crucial organizing feedback. Similarly, this has been found by Yang and Tan (2020) with WRF. For them, the expansion of dry areas was due to the dry-subsidence feedback. Tompkins and Semie (2017), using WRF, found that water vapor feedback with convection is a necessary but not sufficient condition for convective aggregation. Our work, as these results, points out that there are still some disagreements between models in reproducing convective aggregation, as also underlined by (Wing et al., 2020), depending on their physics and numerics.

The ARPS and SAM model reaches their equilibrium in very different ways. We believe that this is the main reason behind their different final equilibrium state of convective organization. In particular, the small domain simulation of ARPS is entirely covered by a large anvil (Figure 1) when reaching its equilibrium. Such an anvil blocks incoming radiation and the simulation domain starts to get colder and drier with a high precipitation rate. When initializing the new large simulation, the cloud water and ice at 12 km are removed, removing the large anvil, while leaving its effect on the vertical profile of temperature and water vapor. Therefore, an aggregated state is obtained, but this occurs in a drier and colder domain, with a nearly saturated sub-cloud layer. The usually adopted procedure of initialization by a small domain (see RCEMIP protocol (Wing et al., 2018)), is thought to eliminate a long spin-up period to reach the model's RCE state without large adjustments (Wing et al., 2018). However, such a procedure could be affected by the presence of a large optically thin clouds anvil, which will dry and cool the whole domain. Such presence is evident also in other models of the RCEMIP project, as shown by large cloud fractions in Figure 9 of Wing et al. (2020).

The reason behind the large anvil cloud fraction and cloud ice in the ARPS small domain simulation has to be found in the microphysics scheme (Lin et al., 1983) and is closely linked to both the ice aggregation process for snow formation and ice sedimen-

tation. Regarding the former process, the threshold for ice aggregation in ARPS is very high, meaning that in ARPS there is less aggregation of ice to form snow, thus leading to the presence of more cloud ice. Furthermore, the sedimentation of ice is removed in ARPS since cloud water and cloud ice are considered to be small enough to have negligible terminal velocities when compared to rain, snow, and graupel. For these reasons, in the small domain simulation of the ARPS model, the cloud water/ice covers the entire domain. Instead, in the SAM model, cloud ice is allowed to fall with its own terminal velocity. In Khairoutdinov and Randall (2003) it was verified that the presence of ice sedimentation in SAM leads to a reduced anvil below 9 km. Thus, in the absence of ice sedimentation, the anvil in SAM would have been more extensive, than the ARPS one. As already mentioned in the previous section, the microphysics differences among the same schemes influence not only the cloud fraction but also the cloud condensate.

The updrafts number and velocity are lower in ARPS than in SAM. They could be diluted by the larger lateral mixing of ARPS (not shown). Following Tompkins and Semie (2017) greater lateral mixing would help the convective organization. The effect of mixing will be investigated in more detail in a following paper. However, we note here that an organized state in SAM is reached with a very small lateral mixing, in contrast to what was predicted by (Tompkins & Semie, 2017). SAM is likely compensating the mixing effect with numerical diffusion due to the second-order accurate advection scheme (Smolarkiewicz & Grabowski, 1990), or the radiative feedback is so strong that aggregation can occur also in an environment where deep convection is not sensitive to entrainment (as occurring in the SAM model).

5 Conclusions

In this study, we performed two RCE simulations with two different CRM (SAM and ARPS) and we compared their properties while reaching a statistical equilibrium of precipitation. This study, like other papers using different models besides SAM to investigate convective organization (Jeevanjee & Romps, 2013; Holloway & Woolnough, 2016; Tompkins & Semie, 2017; Yang & Tan, 2020) point out that there are still some disagreements between models in reproducing convective aggregation, as also underlined by (Wing et al., 2020), depending on their physics and numerics.

The two models, when reaching the organized state, present a warmer and drier domain, with a smaller anvil cloud fraction. Similar findings have been obtained in studies involving idealized 3D simulations (Bretherton et al., 2005; Emanuel et al., 2014; Wing & Emanuel, 2014), in the RCEMIP project (Wing et al., 2020) and in observations (Tobin et al., 2012). On the other hand, during the organization, different feedback are at play. In the SAM model convective organization is achieved due to clouds-radiative feedback (Stephens et al., 2008; C. J. Muller & Held, 2012; Wing & Cronin, 2016), where the presence of a deck of low shallow liquid clouds generates a shallow level circulation which transports MSE up-gradient, making the moist (dry) regions moister (drier). In the ARPS model, instead, the mechanism behind the onset of the convective organization is that of moisture-memory feedback (Tompkins, 2001b; Jeevanjee & Romps, 2013; C. Muller & Bony, 2015), where the convection amplifies in the already moist regions. We found that, with convective organization, in both models, a warmer atmosphere leads to a reduction of the anvil cloud area fraction, the so-called "Iris Effect" (Lindzen et al., 2001; Mauritsen & Stevens, 2015). Indeed, as mentioned above, in both models the anvil cloud fraction decreases with the organization.

We found that the sub-cloud layer properties are very important for the organization, because of their relation with downdrafts and cold pools in the RCE simulations, leading to different feedback between convection and water vapor. This aspect can be different for different models, even if run in a similar setup, as shown in the RCEMIP (Wing et al., 2020). Thus it may have important implications for the convective aggregation in models.

We have measured the convective organization in the two models with the same metrics used in RCEMIP. Although a state of the convective organization is reached by both models, their properties are different. We found that SAM and ARPS differ for the final convective cluster dimensions and type and for the degree of organization. The latter is indicated by the value of the Iorg index, higher for the SAM model than for the ARPS model, meaning a stronger organization for the SAM model compared to the ARPS model. Although the RCE average statistics of ARPS, for some aspects (atmospheric energy imbalance and total heat fluxes) are outside the typical range of RCEMIP models; its degree of aggregation corresponds to the average value for the RCEMIP models.

Different degrees of aggregation and different mechanisms bringing to the convective organization, as found in the two models, have different impacts on the climate system. Therefore, theories about climate sensitivity should always consider different types of models, with respect to their physical and numerical formulation.

Open Research

Data Availability Statement

SAM and ARPS models output used in this manuscript are publicly available via Zenodo. The SAM output is available at https://doi.org/10.5281/zenodo.6949308 and the ARPS output is available at https://doi.org/10.5281/zenodo.6953873.

Acknowledgments

This research has been funded by the Italian Ministry of University and Research (MIUR) and University of Perugia within the program *Dipartimenti di Eccellenza 2018-2022*. The authors thank Ming Xue and Marat Khairoutdinov for providing the ARPS and the SAM models, and Kerry Emanuel for the useful discussion during the development of this work.

References

Bongioannini Cerlini, P., Emanuel, K. A., & Todini, E. (2005). Orographic effects on convective precipitation and space-time rainfall variability: preliminary results. *Hydrology and Earth System Sciences*, *9*(4), 285–299.

Bretherton, C. S., Blossey, P. N., & Khairoutdinov, M. (2005). An energy-balance analysis of deep convective self-aggregation above uniform SST. *Journal of the atmospheric sciences*, *62*(12), 4273–4292.

Chou, M.-D. (1990). Parameterizations for the absorption of solar radiation by o 2 and co 2 with application to climate studies. *Journal of Climate*, *3*(2), 209–217.

Chou, M.-D., & Suarez, M. J. (1994). An efficient thermal infrared radiation parameterization for use in general circulation models. *NASA Technical Memorandum*, *3*, Article ID 104606.

Collins, W. D., Rasch, P. J., Boville, B. A., Hack, J. J., McCaa, J. R., Williamson, D. L., ... Zhang, M. (2006). The formulation and atmospheric simulation of the Community Atmosphere Model version 3 (CAM3). *Journal of Climate*, *19*(11), 2144–2161.

Coppin, D., & Bony, S. (2015). Physical mechanisms controlling the initiation of convective self-aggregation in a general circulation model. *Journal of Advances in Modeling Earth Systems*, *7*(4), 2060–2078.

Craig, G. C., & Mack, J. M. (2013). A coarsening model for self-organization of tropical convection. *Journal of Geophysical Research: Atmospheres*, *118*(16), 8761–8769.

Drager, A. J., & van den Heever, S. C. (2017). Characterizing convective cold pools. *Journal of Advances in Modeling Earth Systems*, *9*(2), 1091–1115.

Emanuel, K., Wing, A. A., & Vincent, E. M. (2014). Radiative-convective instability. *Journal of Advances in Modeling Earth Systems*, *6*(1), 75–90.

Hartmann, D. L., & Berry, S. E. (2017). The balanced radiative effect of tropi-

cal anvil clouds. *Journal of Geophysical Research: Atmospheres*, *122*(9), 5003–5020.

Held, I. M., Hemler, R. S., & Ramaswamy, V. (1993). Radiative-convective equilibrium with explicit two-dimensional moist convection. *Journal of Atmospheric Sciences*, *50*(23), 3909–3927.

Hohenegger, C., & Stevens, B. (2016). Coupled radiative convective equilibrium simulations with explicit and parameterized convection. *Journal of Advances in Modeling Earth Systems*, *8*(3), 1468–1482.

Holloway, C. E., & Woolnough, S. J. (2016). The sensitivity of convective aggregation to diabatic processes in idealized radiative-convective equilibrium simulations. *Journal of Advances in Modeling Earth Systems*, *8*(1), 166–195.

Islam, S., Bras, R. L., & Emanuel, K. A. (1993). Predictability of mesoscale rainfall in the tropics. *Journal of Applied Meteorology and Climatology*, *32*(2), 297–310.

Jeevanjee, N., & Romps, D. M. (2013). Convective self-aggregation, cold pools, and domain size. *Geophysical Research Letters*, *40*(5), 994–998.

Kessler, E. (1969). On the distribution and continuity of water substance in atmospheric circulations. In *On the distribution and continuity of water substance in atmospheric circulations* (pp. 1–84). Springer.

Khairoutdinov, M. F., Blossey, P. N., & Bretherton, C. S. (2022). Global system for atmospheric modeling: Model description and preliminary results. *Journal of Advances in Modeling Earth Systems*. (e2021MS002968 2021MS002968) doi: https://doi.org/10.1029/2021MS002968

Khairoutdinov, M. F., & Emanuel, K. (2010). Aggregated convection and the regulation of tropical climate. In *29th conf. on hurricanes and tropical meteorology* (pp. P2–69).

Khairoutdinov, M. F., Krueger, S. K., Moeng, C.-H., Bogenschutz, P. A., & Randall, D. A. (2009). Large-eddy simulation of maritime deep tropical convection. *Journal of Advances in Modeling Earth Systems*, *1*(4).

Khairoutdinov, M. F., & Randall, D. A. (2003). Cloud resolving modeling of the ARM summer 1997 IOP: Model formulation, results, uncertainties, and sensitivities. *Journal of Atmospheric Sciences*, *60*(4), 607–625.

Lin, Y.-L., Farley, R. D., & Orville, H. D. (1983). Bulk parameterization of the snow field in a cloud model. *Journal of Applied Meteorology and climatology*, *22*(6), 1065–1092.

Lindzen, R. S., Chou, M.-D., & Hou, A. Y. (2001). Does the earth have an adaptive infrared iris? *Bulletin of the American Meteorological Society*, *82*(3), 417–432.

Liou, K.-N. (1986). Influence of cirrus clouds on weather and climate processes: A global perspective. *Monthly Weather Review*, *114*(6), 1167–1199.

Mauritsen, T., & Stevens, B. (2015). Missing iris effect as a possible cause of muted hydrological change and high climate sensitivity in models. *Nature Geoscience*, *8*(5), 346–351.

Muller, C., & Bony, S. (2015). What favors convective aggregation and why? *Geophysical Research Letters*, *42*(13), 5626–5634.

Muller, C., Yang, D., Craig, G., Cronin, T., Fildier, B., Haerter, J. O., ... others (2022). Spontaneous aggregation of convective storms. *Annual Review of Fluid Mechanics*, *54*, 133–157.

Muller, C. J., & Held, I. M. (2012). Detailed investigation of the self-aggregation of convection in cloud-resolving simulations. *Journal of the Atmospheric Sciences*, *69*(8), 2551–2565.

Patrizio, C. R., & Randall, D. A. (2019). Sensitivity of convective self-aggregation to domain size. *Journal of Advances in Modeling Earth Systems*, *11*(7), 1995–2019.

Pauluis, O., & Held, I. M. (2002a). Entropy budget of an atmosphere in radiative–convective equilibrium. part ii: Latent heat transport and moist processes.

Journal of Atmospheric Sciences, *59*(2), 140–149.

Pauluis, O., & Held, I. M. (2002b). Entropy budget of an atmosphere in radiative–convective equilibrium. part i: Maximum work and frictional dissipation. *Journal of the Atmospheric Sciences*, *59*(2), 125–139.

Pope, K. N., Holloway, C. E., Jones, T. R., & Stein, T. H. (2021). Cloud-Radiation Interactions and Their Contributions to Convective Self-Aggregation. *Journal of Advances in Modeling Earth Systems*, *13*(9), e2021MS002535.

Randall, D. A., Hu, Q., Xu, K.-M., & Krueger, S. K. (1994). Radiative-convective disequilibrium. *Atmospheric Research*, *31*(4), 315–327.

Robe, F. R., & Emanuel, K. A. (1996). Moist convective scaling: Some inferences from three-dimensional cloud ensemble simulations. *Journal of Atmospheric Sciences*, *53*(22), 3265–3275.

Ruppert Jr, J. H., & Hohenegger, C. (2018). Diurnal circulation adjustment and organized deep convection. *Journal of Climate*, *31*(12), 4899–4916.

Schlemmer, L., & Hohenegger, C. (2014). The formation of wider and deeper clouds as a result of cold-pool dynamics. *Journal of the Atmospheric Sciences*, *71*(8), 2842–2858.

Schlimme, I., Macke, A., & Reichardt, J. (2005). The impact of ice crystal shapes, size distributions, and spatial structures of cirrus clouds on solar radiative fluxes. *Journal of the Atmospheric Sciences*, *62*(7), 2274–2283.

Semie, A. G., & Bony, S. (2020). Relationship between precipitation extremes and convective organization inferred from satellite observations. *Geophysical Research Letters*, *47*(9), e2019GL086927.

Skamarock, W. C., Klemp, J. B., Dudhia, J., Gill, D. O., Barker, D. M., Wang, W., & Powers, J. G. (2005). *A description of the advanced research wrf version 2* (Tech. Rep.). National Center For Atmospheric Research Boulder Co Mesoscale and Microscale .

Smolarkiewicz, P. K., & Grabowski, W. W. (1990). The multidimensional positive definite advection transport algorithm: Nonoscillatory option. *Journal of Computational Physics*, *86*(2), 355–375.

Sobel, A. H., Bellon, G., & Bacmeister, J. (2007). Multiple equilibria in a single-column model of the tropical atmosphere. *Geophysical Research Letters*, *34*(22).

Stephens, G. L., Van Den Heever, S., & Pakula, L. (2008). Radiative–convective feedbacks in idealized states of radiative–convective equilibrium. *Journal of the Atmospheric Sciences*, *65*(12), 3899–3916.

Sun, S., Zhou, B., Xue, M., & Zhu, K. (2021). Scale-similarity subgrid-scale turbulence closure for supercell simulations at kilometer-scale resolutions: Comparison against a large-eddy simulation. *Journal of the Atmospheric Sciences*, *78*(2), 417–437.

Tobin, I., Bony, S., & Roca, R. (2012). Observational evidence for relationships between the degree of aggregation of deep convection, water vapor, surface fluxes, and radiation. *Journal of Climate*, *25*(20), 6885–6904.

Tompkins, A. M. (2001a). Organization of tropical convection in low vertical wind shears: The role of cold pools. *Journal of the atmospheric sciences*, *58*(13), 1650–1672.

Tompkins, A. M. (2001b). Organization of tropical convection in low vertical wind shears: The role of water vapor. *Journal of the atmospheric sciences*, *58*(6), 529–545.

Tompkins, A. M., & Craig, G. C. (1998). Radiative–convective equilibrium in a three-dimensional cloud-ensemble model. *Quarterly Journal of the Royal Meteorological Society*, *124*(550), 2073–2097.

Tompkins, A. M., & Semie, A. G. (2017). Organization of tropical convection in low vertical wind shears: Role of updraft entrainment. *Journal of Advances in Modeling Earth Systems*, *9*(2), 1046–1068.

Windmiller, J. M., & Craig, G. C. (2019). Universality in the spatial evolution of self-aggregation of tropical convection. *Journal of the Atmospheric Sciences*, *76*(6), 1677–1696.

Wing, A. A., & Cronin, T. W. (2016). Self-aggregation of convection in long channel geometry. *Quarterly Journal of the Royal Meteorological Society*, *142*(694), 1–15.

Wing, A. A., Emanuel, K., Holloway, C. E., & Muller, C. (2017). Convective self-aggregation in numerical simulations: A review. *Shallow clouds, water vapor, circulation, and climate sensitivity*, 1–25.

Wing, A. A., & Emanuel, K. A. (2014). Physical mechanisms controlling self-aggregation of convection in idealized numerical modeling simulations. *Journal of Advances in Modeling Earth Systems*, *6*(1), 59–74.

Wing, A. A., Reed, K. A., Satoh, M., Stevens, B., Bony, S., & Ohno, T. (2018). Radiative–convective equilibrium model intercomparison project. *Geoscientific Model Development*, *11*(2), 793–813.

Wing, A. A., Stauffer, C. L., Becker, T., Reed, K. A., Ahn, M.-S., Arnold, N. P., ... Zhao, M. (2020). Clouds and convective self-aggregation in a multimodel ensemble of radiative-convective equilibrium simulations. *Journal of Advances in Modeling Earth Systems*, *12*(9), e2020MS002138.

Xue, M., Droegemeier, K. K., & Wong, V. (2000). The Advanced Regional Prediction System (ARPS)–A multi-scale nonhydrostatic atmospheric simulation and prediction model. Part I: Model dynamics and verification. *Meteorology and Atmospheric Physics*, *75*(3), 161–193.

Xue, M., Droegemeier, K. K., Wong, V., Shapiro, A., Brewster, K., Carr, F., ... Wang, D. (2001). The advanced regional prediction system (arps)–a multi-scale nonhydrostatic atmospheric simulation and prediction tool. part ii: Model physics and applications. *Meteorology and atmospheric physics*, *76*(3), 143–165.

Xue, M., Hu, M., & Schenkman, A. D. (2014). Numerical prediction of the 8 May 2003 Oklahoma City tornadic supercell and embedded tornado using ARPS with the assimilation of WSR-88D data. *Weather and Forecasting*, *29*(1), 39–62.

Yang, B., & Tan, Z.-M. (2020). The initiation of dry patches in cloud-resolving convective self-aggregation simulations: Boundary layer dry-subsidence feedback. *Journal of the Atmospheric Sciences*, *77*(12), 4129–4141.